

NMR spectroscopy and conformational analysis of 3-deoxy-3-*C*-(hydroxymethyl)-1,2:5,6-di-*O*-isopropylidene- α -D-allofuranose

David C. Lankin ^{a,*}, Sean T. Nugent ^b and Shashidhar N. Rao ^c

^a Physical Methodology Department, ^b Chemistry Department, ^c Drug Design,
Searle Research & Development 4901 Searle Parkway, Skokie, Illinois 60077 (USA)

(Received July 19th, 1992; accepted in revised form December 30th, 1992)

ABSTRACT

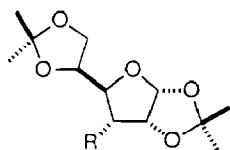
Homonuclear and heteronuclear 1- and 2-dimensional NMR techniques have been used to establish stereochemical and conformational relationships in the hydroxymethyl furanoside **2**. Concurrent with the NMR studies, theoretical calculations were performed on this compound using computer-assisted model building (MacroModel) and molecular mechanics (MM2). From the NOE and *J*-coupling constraints obtained from NMR experiments, refined structures for this compound in two different solvents have been identified and optimized. The “solvent effects” observed in the NMR spectra for **2** are interpreted in terms of the differences in the requirements for intramolecular electrostatic stabilization in the two solvents.

INTRODUCTION

In an earlier paper¹, we reported the results of NMR experiments and theoretical calculations on 3-*C*-(cyanomethyl)-3-deoxy-1,2:5,6-di-*O*-isopropylidene- α -D-allofuranose (**1**). Therein we qualitatively correlated the model-built and energy-refined structures with ¹H NMR coupling constants and nuclear Overhauser effects (NOEs) leading to a confirmation of the structure and solution dynamics of **1**.

As a continuation of our interest in compounds containing this ring system, we report here a detailed study, using a similar combination of NMR spectroscopy and computational techniques, of the structure and stereochemistry of 3-deoxy-3-*C*-(hydroxymethyl)-1,2:5,6-di-*O*-isopropylidene- α -D-allofuranose⁴ (**2**). The results obtained¹ for **1** provided a unified qualitative correlation of NMR results and calculations in a system in which strong intramolecular electrostatic interactions were absent. The potential for intramolecular hydrogen bonding in **2**, however, is

* Corresponding author.

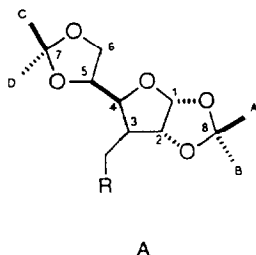


1 : R = CH₂CN

2: R = CH₂OH

expected to evoke changes in the conformational dynamics of this carbohydrate ring system relative to **1**. The present study describes solution NMR investigations on **2** in CDCl₃ and Me₂SO-*d*₆ and the correlation of these results with theoretical calculations.

For clarity, we have employed, in conjunction with the standard numbering for the furanose ring system **A**, the following numbering and lettering scheme which denotes the pendant and fused *O*-isopropylidene quaternary carbons as C-7 and C-8, respectively. The methyl groups attached to C-8 are denoted as Me(A) and Me(B) with Me(A) being *syn* to protons H-1 and H-2. The methyl groups attached to C-7 are denoted as Me(C) and Me(D) with Me(C) being *syn* to protons H-5 and H-6 and with Me(D) being *syn* to H-6'.

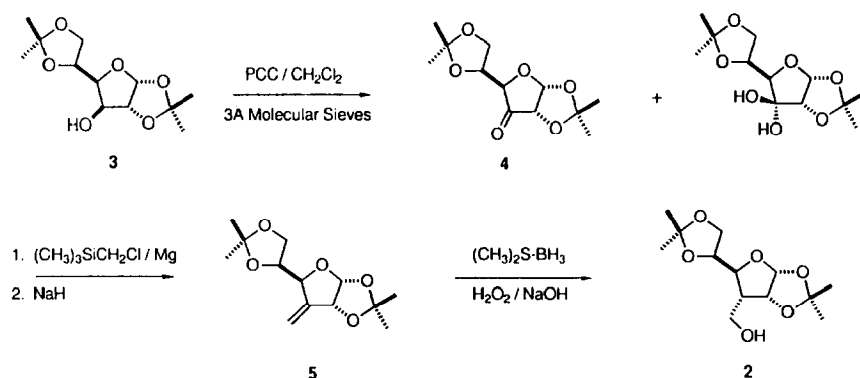


A

RESULTS AND DISCUSSION

Synthesis.—Compound **2** was prepared from readily available 1,2:5,6-di-*O*-isopropylidene- α -D-glucofuranose (**3**, Scheme 1). Oxidation of **3** with pyridinium chlorochromate (PCC) in the presence of pulverized 3A molecular sieves afforded a 60:40 mixture of 1,2:5,6-di-*O*-isopropylidene- α -D-ribo-hexofuranos-3-ulose⁵ (**4**) and its hydrate. Treating this mixture with the Grignard reagent from trimethylsilylmethylmagnesium chloride in refluxing THF afforded the silyl alcohol² (85%), which was immediately subjected to Peterson fragmentation³ affording the exocyclic enose **5** in 82% yield for the two steps. Hydroboration of **5** with borane–dimethyl sulfide complex afforded the desired branched allose **2** in 78% yield.

The hydroboration of the double bond in **5** can occur from either the α - or β -face leading to two possible epimeric hydroxymethyl products, **2** or **epi-2**. Results



Scheme 1.

from the NMR experiments (*vide infra*) clearly indicate the product of this reaction to be **2**, which arises from delivery of hydride to the β -face of **5**. This result is consistent with qualitative predictions based on steric criteria, the known mechanism of hydroboration, and further parallels the stereochemical outcome of the catalytic hydrogenation reaction¹ used to produce the structurally related **1**.

NMR studies: proton NMR resonance assignments.—The proton NMR assignments for **2** in CDCl_3 and $\text{Me}_2\text{SO}-d_6$ were confirmed using 1- and 2-dimensional NMR techniques. The assignment of the proton NMR spectra for **2** in CDCl_3 follows from the interpretation of the phase-sensitive double-quantum filtered COSY (DQF-COSY)⁵ data together with the phase-sensitive (NOESY)⁶ data. The assignments of the proton chemical shifts and coupling constants for the six overlapped and congested protons H-3'(A), H-3'(B), H-4, H-5, H-6, and H-6' were evaluated from the homonuclear 2D J -spectra obtained for **2** in CDCl_3 . The proton NMR spectrum obtained for **2** in $\text{Me}_2\text{SO}-d_6$ was less congested and consisted of overlapped nearly first-order spin patterns. Assignment of the OH-3' resonance for **2** in each of the two solvents was confirmed by D_2O exchange experiments, the results of which also served to simplify, in particular, the spin patterns for H-3'(A) and H-3'(B). The geminal methyl pairs Me(A)–Me(B) and Me(C)–Me(D) which are attached to the same quaternary carbons C-8 and C-7, respectively, were unambiguously assigned from the COSY and NOESY spectra for both solvents. The COSY data reveals cross-peaks arising from the 4-bond coupling between the methyl groups attached to the same carbon atom. These assignments were critically important for the subsequent conformational studies. Tables I and II summarize the proton chemical shifts and coupling constants obtained for **2** in both solvents. The combined use of proton homonuclear 2D NMR techniques described herein affords the necessary information leading to a self-consistent assignment of all of the proton chemical shifts for **2**.

The phase-sensitive NOESY data for **2** corroborates the proton assignments made from the COSY data and reveals important structural details about both the

TABLE I
Proton (400 MHz) chemical-shift data for **2**

Proton assignments ^a	Solvent		$\Delta \delta$ ^b
	CDCl ₃	Me ₂ SO- <i>d</i> ₆	
H-1	5.772 d	5.728 d	+0.044
H-2	4.755 dd	4.685 dd	+0.070
H-3	2.119 ddt	1.966 dddd	+0.153
H-3'(A)	3.911 ddd	3.632 ddd	+0.279
H-3'(B)	3.864 ddd	3.571 ddd	+0.293
H-4	3.895 dd	3.690 br dd	+0.205
H-5	3.990 ddd	4.079 dt	-0.089
H-6	4.157 dd	3.966 dd	+0.191
H-6'	4.021 dd	3.739 dd	+0.282
Me(A)	1.316 s	1.254 s	+0.062
Me(B)	1.518 s	1.400 s	+0.118
Me(C)	1.369 s	1.259 s	+0.110
Me(D)	1.455 s	1.304 s	+0.151
3'-OH	3.280 dd	4.577 dd	-1.297

^a Chemical shifts are expressed in ppm relative to tetramethylsilane (Me₄Si, 0.000 ppm) used as an internal standard. Proton assignments were confirmed by 2-dimensional NMR experiments (DQ-COSY and NOESY). ^b Defined as: δ CDCl₃ - δ Me₂SO-*d*₆.

conformational disposition of the pendant hydroxymethyl group at C-3 as well as contrasting the differences in ring stereochemistry which are evident from the NMR data in the two solvents. In CDCl₃, intramolecular hydrogen bonds between OH-3' and O-2 or O-5 within the molecule are both conformationally possible, while in Me₂SO-*d*₆, intermolecular hydrogen bonding of OH-3' to the solvent competes favorably with the intramolecular hydrogen bonding sites and is expected to predominate.

TABLE II
Proton-proton coupling constants ^a for **2**

Proton assignments	Solvent	
	CDCl ₃	Me ₂ SO- <i>d</i> ₆
<i>J</i> _{1,2}	4.0	3.5
<i>J</i> _{2,3}	4.8	4.5
<i>J</i> _{3,3'(A)}	4.7	5.8
<i>J</i> _{3,3'(B)}	6.9	8.9
<i>J</i> _{3'(A),3'(B)}	-11.9	-10.5
<i>J</i> _{3'(A),OH}	9.7	5.5
<i>J</i> _{3'(B),OH}	3.3	5.4
<i>J</i> _{3,4}	9.6	10.2
<i>J</i> _{4,5}	8.2	5.9
<i>J</i> _{5,6}	5.8	6.4
<i>J</i> _{5,6'}	4.9	5.9
<i>J</i> _{6,6'}	-8.4	-8.2

^a Coupling constants are expressed in Hz. The sign of the geminal coupling constants is inferred.

TABLE III

Carbon-13 (100 MHz) chemical shift data for **2**

Carbon assignments	Solvent		$\Delta \delta^b$
	CDCl_3	$\text{Me}_2\text{SO}-d_6$	
C-1	104.8	104.6	+0.2
C-2	82.4	80.8	+1.6
C-3	51.3	49.9	+1.4
C-3'	59.5	56.8	+2.7
C-4	81.6	79.0	+2.6
C-5	77.1	76.8	+0.3
C-6	67.9	65.6	+2.2
C-7	109.8	108.5	+1.3
C-8	112.2	110.9	+1.9
Me(A)	26.1	26.3	-0.2
Me(B)	26.7	26.8	-0.1
Me(C)	25.1	26.3	-0.2
Me(D)	26.5	25.1	+1.4

^a Chemical shifts are expressed in ppm relative to tetramethylsilane (Me_4Si 0.00 ppm) used as an internal standard. Protonated carbon assignments were confirmed by 2-dimensional NMR (HETCOR).

^b Defined as: $\delta \text{CDCl}_3 - \delta \text{Me}_2\text{SO}-d_6$.

Carbon-13 NMR: resonance assignments.—The ^{13}C NMR assignments for the protonated carbon resonances in **2** follow from the results of the attached proton test (APT)⁷ and the proton–carbon heteronuclear shift correlation (HETCOR)⁸ experiments. Assignment of the quaternary carbon resonances C-7 and C-8 follows analogously by comparison of the carbon shifts for **2** with that of **1** (ref. 1) and related compounds. Table III summarizes the carbon-13 chemical shifts and their assignments for **2** in CDCl_3 and $\text{Me}_2\text{SO}-d_6$.

Conformational and structural aspects.—The 2-dimensional proton NOESY spectrum (Fig. 1A) allows conclusions to be drawn regarding the conformation of **2** in CDCl_3 solution. In this as well as our previous study¹, NOE intensities are arbitrarily assigned as “strong” (s), “medium” (m), and “weak” (w) and correspond to the ranges of distances 1.8 to 2.0, 2.0 to 3.0, and 3.0 to 4.0 Å, respectively. NOE intensities which are not observed correspond to distances > 4.0 Å. The relative intensities of NOESY cross-peaks were evaluated from the 2D contours based on both visual comparisons of the intensities of the geminal and vicinal NOESY cross-peaks relative to cross-peaks corresponding to longer-range dipolar interactions as well as the relative intensity information obtained from slices of the NOESY contour plots. Medium intensity cross-peaks are observed between the vicinally related H-1 and H-2, H-2 and H-3, and H-5 and H-6, whereas strong cross-peaks are observed between the geminally related H-3'(A) and H-3'(B), and H-6 and H-6'. A medium-intensity cross-peak is observed between H-3 and H-5. Weak cross-peaks were observed between Me(A) and both ring protons H-1 and H-2, Me(C) and both H-5 and H-6, Me(D) and H-6' and H-4, and Me(B) and H-4 (Fig. 1B). Weak cross-peaks were also observed between Me(D) and OH-3' as well

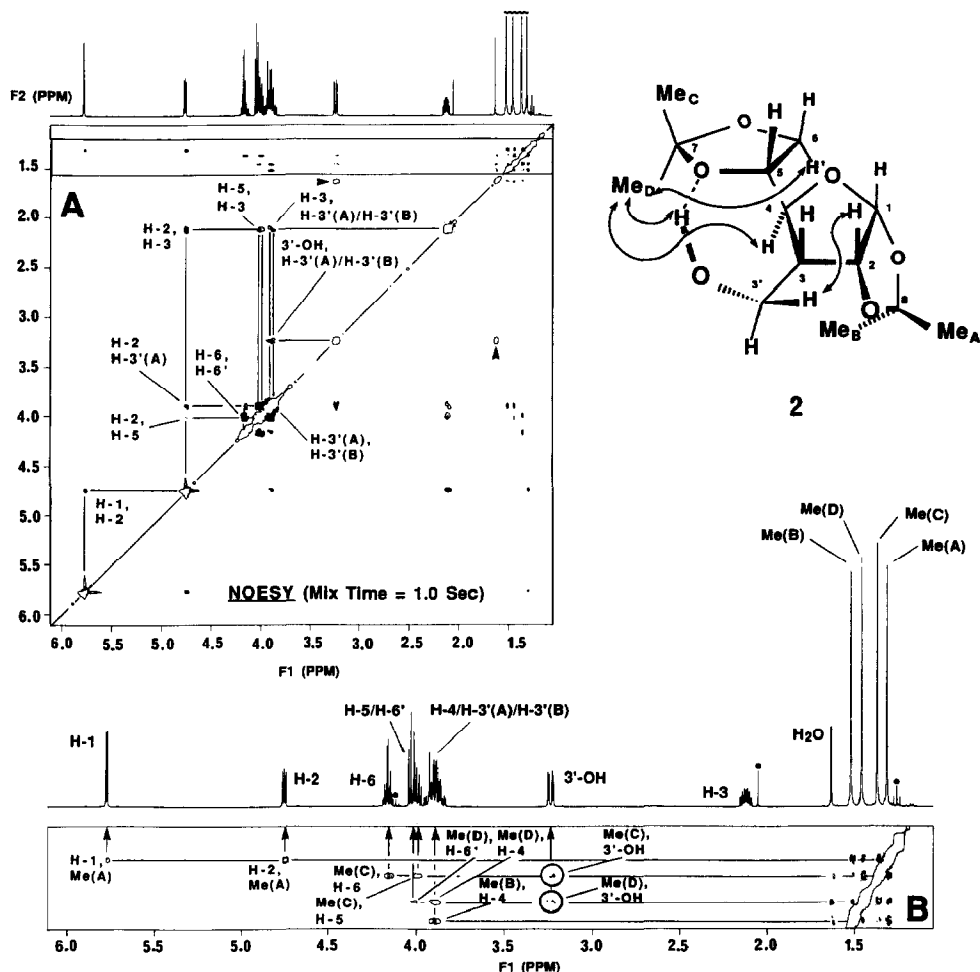


Fig. 1. Phase-sensitive NOESY NMR spectrum for **2** in CDCl_3 solution. (A) Full spectrum. (B) Expansion of the boxed region in (A) showing the correlation cross-peaks between the methyl resonances and the ring protons. Peaks in (A), denoted by (\blacktriangleright), are in-phase cross-peaks characteristic of chemical exchange of OH-3' with the water present in the solvent. Peaks in (B), denoted by (\bullet), indicate trace amounts of ethyl acetate. Key NOE observations are denoted by arrows on the structure for **2** consistent with the NMR results.

as H-2 with *only one of the protons at C-3', H-3'(B)*. The conformation for **2** consistent with the 2D NOESY data in CDCl_3 , which implies the existence of an intramolecular hydrogen bond between OH-3' and O-5, together with key observed NOE interactions is shown in Fig. 1.

Similar to the results obtained for **2** in CDCl_3 , the NOESY data obtained for **2** in $\text{Me}_2\text{SO}-d_6$ (Fig. 2A) also show the weak cross-peaks associated with Me(A) and protons H-1 and H-2, Me(B) and H-4, Me(C) and proton H-5 and H-6, and Me(D) and H-6' (Fig. 2B) as well as the expected medium intensity cross-peaks between the vicinally related H-1 and H-2, H-2 and H-3, H-5 and H-6, and the strong

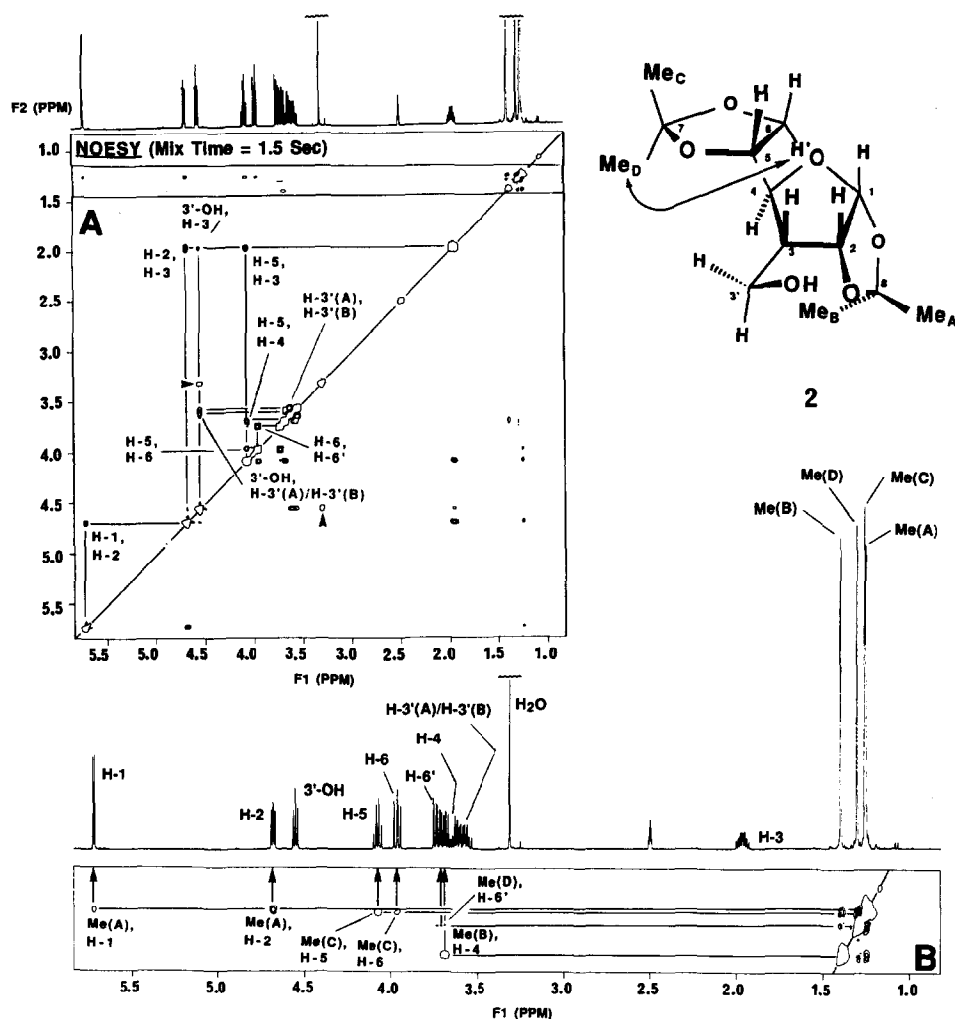


Fig. 2. Phase-sensitive NOESY NMR spectrum for **2** in $\text{Me}_2\text{SO}-d_6$ solution. (A) Full spectrum. (B) Expansion of the boxed region in A showing the correlation cross-peaks between the methyl resonances and the ring protons. Peaks in (A), denoted by (▶), are in-phase cross-peaks characteristic of chemical exchange of OH-3' with the water present in the solvent.

cross-peaks between the geminal protons H-3'(A) and H-3'(C), H-6 and H-6', and H-5 and H-6. Medium intensity cross-peaks between OH-3' and C-3' protons, and between H-5 and H-4 are also observed. Weak cross-peaks are observed between H-3 and OH-3' of the pendant hydroxymethyl group with nearly equal 3-bond couplings being observed between OH-3' and the C-3' protons. Absent from the $\text{Me}_2\text{SO}-d_6$ data, however, is a cross-peak corresponding to a Me(D) to H-4 interaction and an examination of the vicinal coupling constants (Table II) between H-4 and H-5 protons indicate that this value differs from the corresponding value for **2** obtained in CDCl_3 . These latter observations suggest that the orienta-

tion of the hydroxymethyl moiety about the C-3–C-3' bond and the conformational disposition of the 5,6-*O*-isopropylidene ring about the C-4–C-5 bond are clearly different in the two solvent environments.

Molecular modeling.—Concurrent with the NMR studies, the energetically favored structures of **2** were investigated by molecular mechanics. The numbers of conformations within 7 kcal/mol of the global minimum, obtained at the dielectric values of 1.0 and 10.0 were 41 and 29, respectively. The two sets of conformations show significant differences since intramolecular electrostatic stabilizations are feasible in **2** and these are emphasized to different extents in the two dielectrics. Further, conformational energy calculations were also performed wherein energies were evaluated as a function of the torsions about the C-4–C-5 (χ_1) and C-3–C-3' (χ_2) bonds. These computations were carried out with both the MM2 and MM3 force fields (*vide infra*), the latter being known to be better parameterized for carbohydrates^{9,10}.

The models obtained at the dielectric of 1.0 are compared with the NMR data for **2** in CDCl₃. The rationale for this comparison is that the OH-3' is unlikely to be involved in extensive hydrogen bonding with the CDCl₃ and, hence, its structure is likely to be stabilized by intramolecular interactions such as hydrogen bonding. These interactions are better modeled at the lower dielectric. The models obtained at the dielectric of 10.0 will be compared with the NMR data obtained for **2** in Me₂SO-*d*₆, which is capable of forming intermolecular hydrogen bonds with **2**. This results in the disruption of the intramolecular stabilization for **2** observed in CDCl₃. Table IV lists models which lie within 3 kcal/mol of the respective global minima in the two sets along with their relative energies. Figs. 3 and 5 present computer graphics illustrations of some of the energy-refined models obtained at the dielectrics of 1.0 and 10.0, respectively. The terms “around” and “approximately” used herein refer to deviations of no more than 0.1 Å in the case of calculated distances and not more than 10% in the case of torsion angles.

Models at dielectric of 1.0.—Only one conformation (DE1–M2) is found within 1 kcal/mol of the global minimum (DE1–M1) while seventeen are found within 3 kcal/mol of the latter. In both (DE1–M1) and (DE1–M2), OH-3' forms an intramolecular hydrogen-bond with O-5 of the 5,6-*O*-isopropylidene ring (Fig. 3a). The two models are very similar in the fused bicyclic part of **2**, and differ in only the ring geometry of the 5,6-*O*-isopropylidene moiety (Fig. 3a). The model DE1–M3 (Fig. 3b; Table IV) is, however, characterized by a hydrogen bond between the OH-3' and O-2 of the 1,2-*O*-isopropylidene ring. It overlaps with DE1–M1 with an rms deviation of 0.1 Å for the positions of all heavy atoms with the exception of the OH-3' oxygen (Fig. 3b). The model DE1–M4 is characterized by the lack of an intramolecular hydrogen-bond (Fig. 3c) and is energetically destabilized by 1.4 kcal/mol relative to DE1–M1, the global minimum. With the exception of the OH-3', this model overlaps to within 0.1 Å of DE1–M1 and DE1–M3. The NMR data (*vide supra*) is consistent with both (DE1–M1) and (DE1–M2). Of the 16 models which lie between 1 and 3 kcal/mol of the global minimum, 8 have

TABLE IV

Energies (kcal/mol) relative to global minimum of the minimized structures of **2** within 3 kcal/mol at the dielectric of (a) 1.0 and (b) 10.0

a		b	
Model	Energy	Model	Energy
DE1-M1	0.00	DE10-M1	0.00
DE1-M2	0.56	DE10-M2	0.04
DE1-M3	1.19	DE10-M3	0.15
DE1-M4	1.38	DE10-M4	0.15
DE1-M5	1.55	DE10-M5	0.39
DE1-M6	1.70	DE10-M6	0.44
DE1-M7	1.79	DE10-M7	0.81
DE1-M8	2.02	DE10-M8	0.82
DE1-M9	2.03	DE10-M9	0.82
DE1-M10	2.11	DE10-M10	0.85
DE1-M11	2.26	DE10-M11	0.90
DE1-M12	2.54	DE10-M12	0.94
DE1-M13	2.75	DE10-M13	1.10
DE1-M14	2.81	DE10-M14	1.13
DE1-M15	2.82	DE10-M15	1.50
DE1-M16	2.86	DE10-M16	1.52
DE1-M17	2.95	DE10-M17	1.58
DE1-M18	3.00	DE10-M18	1.64
		DE10-M19	1.81
		DE10-M20	2.13
		DE10-M21	2.27

intramolecular hydrogen-bonding interactions similar to that in DE1-M3, while the others are not characterized by either hydrogen bonds or any intramolecular electrostatic stabilization involving OH-3'.

Protons H-1 and H-2 are nearly eclipsed with the torsion angle about the C-1-C-2 bond varying between -5 and -9° in all of the energy-optimized structures. This range is similar to the one obtained for **1** in our previous study¹. As noted earlier¹, the coupling constant $J_{1,2}$ calculated from the energy-minimized models using the method of Haasnoot et al.¹¹ deviates from the experimental observation by ~ 1.5 Hz. Such a difference could be attributed to the stereoelectronic environment present in **2**, which is not taken into account by the Haasnoot relationship.

As in the case of **1**, the dihedral angle H-1-C-2-C-3-H-3 is $40 \pm 1^\circ$ in all the energy-refined models of **2**. This value is consistent with the experimental observation of 4.8 Hz (Table IV) which deviates from the corresponding value for **1** by 0.2 Hz. The torsion angle H-4-C-4-C-3-H-3 is around -170° in **2**, consistent with the NMR observed coupling constant of 9.6 Hz.

The coupling constants between H-3-H-3'(A) and H-3-H-3'(B) are 4.7 and 6.9 Hz, respectively. These values imply neither a pure *gauche* nor a pure *anti* conformation for H-3'(A) and H-3'(B) relative to H-3. These values may also be

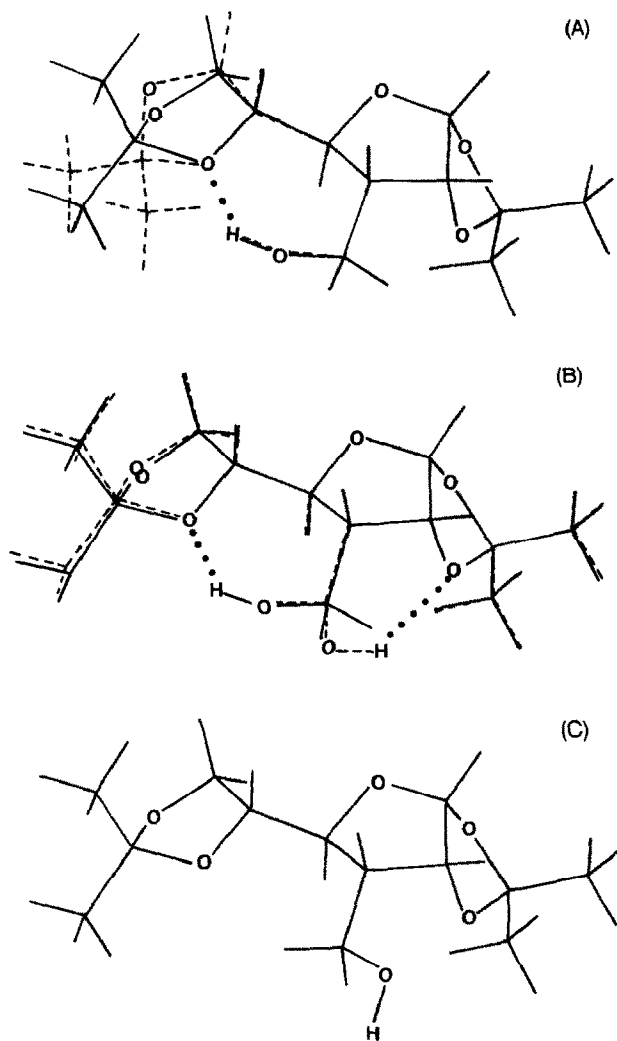


Fig. 3. Computer graphics illustrations of (A) overlap of DE1-M1 (—) and De1-M2 (-----), (B) overlap of De1-Me1 (—) and De1-M3 (-----), and (C) DE1-M4.

contrasted with the corresponding values of 3.7 and 11.2 Hz obtained for **1**. In the refined models of **2**, torsion angles about the C-3-C-3' bond are spread over the *anti* ($\sim 180^\circ$), *gauche*⁺ ($\sim 60^\circ$), and *gauche*⁻ ($\sim -60^\circ$) ranges. The torsion angles H-3-C-3-C-3'-H-3'(A) and H-3-C-3-C-3'-H-3'(B) are around -74° and 165° in both DE1-M1 and DE1-M2, respectively. These two torsions are consistent *qualitatively* (although not *quantitatively*) with the observed coupling constants. The Haasnoot relationship as implemented in MacroModel *does not permit* the calculation of coupling constants for the H-3 and H-3'(A or B) protons due to the presence of the OH-3' group. Further, this relationship is an approximation that

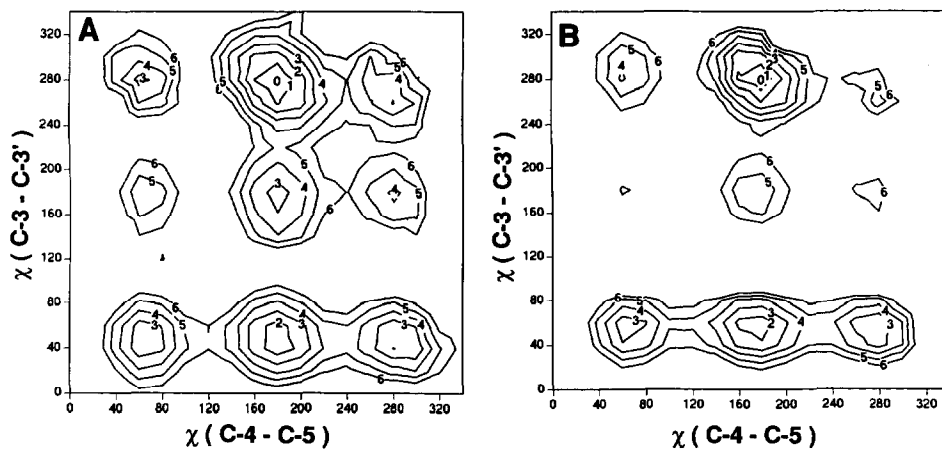


Fig. 4. Energy plots of **2** in the conformational space of the torsions about the C-3–C-3' (Y-axis) and C-4–C-5 (X-axis) bonds, with MM2 (A) and MM3 (B) force fields. Isoenergy contours are drawn at 1 kcal/mol intervals starting from the global minimum (marked 0). See text for details.

does not take into account the presence of explicit solvation, solute concentration, and so on. Accordingly, the significance of the torsions in the theoretical models in relationship to the observed coupling can at best be considered *qualitative*. The larger coupling constant of 6.9 for H-3'(B) suggests a more extended conformation than for H-3'(A) and this is borne out in our models for **2**. The results of the exhaustive conformational energy calculations (Fig. 4) clearly suggest that the C-3–C-3' torsion is flexible implying that the hydroxymethyl group spends some of its time in conformations other than the global minimum. The values of the observed coupling constants do suggest that the latter conformation plays a significant role in deciding the average conformation about the C-3–C-3' bond. Two other models (DE1–M12 and DE1–M14) also have similar values of these torsions. However, the latter two structures have energies of more than 2 kcal/mol relative to the global minimum (Table IV).

The torsion angle H-4–C-4–C-5–H-5 which defines the orientation of the 5,6-*O*-isopropylidene ring relative to the [3.3.0] ring system is predominantly between 175 and 185° in all the energy-refined models of **1** which lie within 2 kcal/mol of the global minimum. The calculated *J* values for these models lie in the range 9.2–9.4 ± 1.0 Hz. In models whose relative energies are 2 kcal/mol greater, this torsion adopts either a *gauche*⁺ (~ 60°) or a *gauche*⁻ (~ -60°) value. The observed H-4–H-5 coupling of 8.2 Hz in CDCl₃ (Table IV) is once again *qualitatively* consistent with the values of ~ 180° for torsions about C-4–C-5. This value corresponds to a torsion of ~ 155° about C-4–C-5 and as noted from the contour plots (Fig. 4), such a value lies within 2 kcal/mol of the global minimum. This observed “average” conformation could be visualized as arising from the major contributions from the predominately *anti* conformations as well as from minor contributions from the *gauche* conformations both of which lie within

3 kcal/mol of the global minimum. These contributions can be rationalized on the basis of the energy plots in Fig. 4 wherein a larger area is enclosed by 3 kcal/mol contours at around the *anti* values of the C-4–C-5 conformation as compared to the corresponding *gauche* values.

The geometries of the 5,6-*O*-isopropylidene ring in DE1–M1 and DE1–M2 are significantly different, although both structures have an internal hydrogen bond between OH-3' and O-5. This ring has envelope conformations in both the models. In DE1–M1, the atoms O-5, C-5, C-6, and O-6 are coplanar with C-7 puckered out of the plane, while in DE1–M2, O-6 is puckered out of the plane formed by the other four atoms. The torsion angles for the four coplanar atoms in each of the two models are less than 1°. The envelope form of this ring system is also observed in DE1–M3 and DE1–M4. The former has an intramolecular hydrogen bond between OH-3' and O-2 in the 1,2-*O*-isopropylidene ring, while the latter has no intramolecular hydrogen bonds. The 5,6-*O*-isopropylidene ring in other DE1 models has a twist conformation rather than an envelope.

The calculated vicinal coupling constants $J_{5,6}$ and $J_{5,6'}$ in DE1–M1 and DE1–M2 are significantly different to those observed by NMR studies (5.8 and 4.9 Hz, respectively). The calculated values are 8.7 and 7.1 Hz in DE1–M1 and 7.3 and 10.2 Hz in DE1–M2, respectively. These differences could be attributed to variations of the ring geometry in the calculated models and experimental conditions (solvation effects). Further, the observed geminal coupling constants between H-6 and H-6' differ significantly from $J_{3'(A),3'(B)}$ implying possible influence of bond angle strain in the 5,6-*O*-isopropylidene ring. In the molecular modeling calculations, we have allowed bond angles to relax without any constraints. In other words, the bond angles were not systematically varied as were some of the torsion angles (see Experimental section). Since the bond angles in the energy refined models correspond only to fully optimized situations, their influence on coupling constants at other values can not be estimated. In addition to possible bond angle effects, electronegativity effects, not explicitly included in our calculations, could account for some of the differences between the calculated and observed coupling constants associated with the 5,6-*O*-isopropylidene ring. Such effects are known to affect geminal couplings in a variety of molecular systems^{12–14*,15}.

The coupling observed for **2** are similar to and consistent with the data reported earlier¹⁶ for the 1,2:5,6-di-*O*-isopropylidene- α -D-allofuranose (R = OH in **2**). Two exceptions to this data were found in the case of couplings between H-3–H-4 (8.6 vs. 9.6 Hz) and H-4–H-5 (4.8 vs. 8.2 Hz). These differences can be accounted for by the fact that the substituent in the α position at C-3 (i.e., –OH) differs by a methylene group. This in turn introduces both electronegativity and conforma-

* We would like to thank one of the referees for “re-acquainting” us with this most extensive of studies.

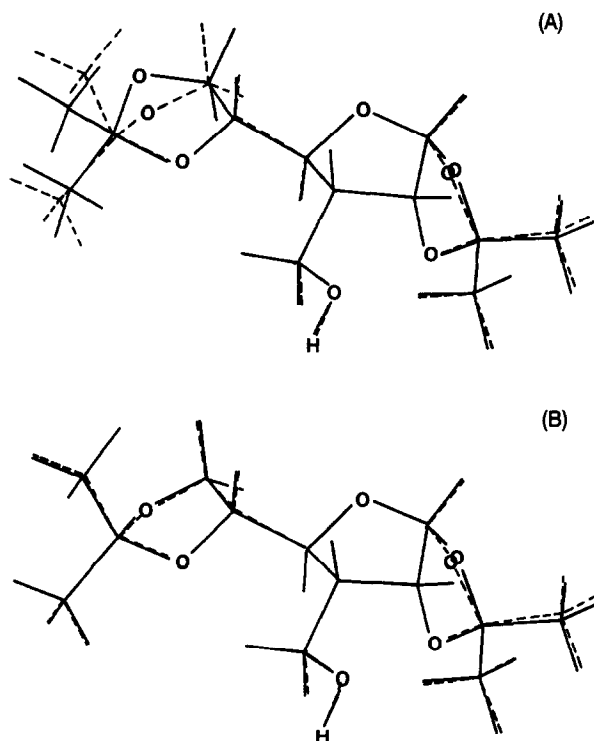


Fig. 5. Computer graphics illustrations of (A) overlap of DE10-M1 (—) and DE1-M4 (-----), and (B) overlap of DE10-M2 (—) and DE1-M4 (-----).

tional effects which could potentially serve to alter the magnitude of the couplings. These differences in coupling constants are also paralleled by the corresponding chemical shifts which differ significantly only in the chemical shifts of H-3 and H-5. The impact of the hydroxyl vs. hydroxymethyl substituents at C-3 on the molecular structure of 1,2:5,6-di-*O*-isopropylidene derivatives is being investigated theoretically in our laboratory and will be reported in due course.

Models at dielectric of 10.0.—All the models obtained for **2** are devoid of any intramolecular electrostatic stabilizations as OH-3' is pointed away from both isopropylidene rings in all cases. Interestingly, these models are qualitatively very similar to DE1-M4 which also lacked intramolecular stabilizations (*vide infra*). Fig. 5 illustrates the overlaps of DE10-M1 and DE10-M2 with DE1-M4 which demonstrate the structural similarity of these models. A dozen models have energies within 1 kcal/mol of the global minimum (Table IV) while twenty-one models have energies within 3 kcal/mol of the global minimum.

As in the case of DE1 models, the protons H-1 and H-2 are nearly eclipsed with the torsion angle about the C-1–C-2 bond varying between -10.5 and -11° in all of the energy-optimized structures. The calculated $J_{1,2}$ in the energy-minimized models (~ 5.4 Hz) using the method of Haasnoot deviates from the experimental observation by ~ 1.9 Hz. The torsion between H-3 and H-4 is *anti* in all the

energy-minimized models. Further, as in DE1 models and in models of **1**, the H-2–C-2–C-3–H-4 torsions are all $\sim 40^\circ$.

The torsion angle H-4–C-4–C-5–H-5 is confined mainly to *gauche*⁺ and *anti* values in the top twelve structures which lie within 1 kcal/mol of the global minimum. The observed NMR coupling constant, $J_{4,5}$ is 5.9 Hz and taken together with the molecular modeling results is indicative of a mixture of populations *non-trivially* biased by the *gauche*⁺ conformation. The presence of multiple conformations of unequal populations can complicate interpretation of the NOE data in terms of extracting exact distance information from the NMR data in that it invalidates the “one-NOE:one distance” approximation. This results in an NMR derived solution structure in which the distances obtained are conformationally averaged. Recently, Landis and Allured¹⁷ introduced the conformer population analysis (CPA) protocol for quantitatively extracting accurate proton internuclear distance information from NOESY data for a variety of conformationally mobile small molecules. Such methodology directly employs the NOE intensities and is predicted to give better results than the distance constrained methods for evaluating interatomic distances and molecular structures. However, it is suggested that the CPA approach is sensitive to the method of generation of the energetically feasible molecular conformations¹⁷. In our laboratory, studies combining the CPA approach together with molecular dynamics simulations applied to **1** and **2** are currently in progress in an effort to provide a more quantitative correlation of the observed NOE intensities with the theoretically calculated models and will be reported separately.

Quantitatively consistent with the NMR coupling constants of 5.8 and 8.9 Hz for $J_{3,3'(A)}$ and $J_{3,3'(B)}$ (Table II), the torsions H-3–C-3–C-3'–H-3'A and H-3–C-3–C-3'–H-3'(B) are either *gauche* or *anti* in DE10–M1 through DE10–M12. This suggests the possibility of hindered rotation about the C-3'–C-3 bond since the OH-3' is no longer hydrogen-bonded to any of the isopropylidene ring oxygens. As noted earlier, this situation mimics the most probable scenario in the presence of Me₂SO-*d*₆ as the solvent.

For all models within 1 kcal/mol of the global minimum, the conformations of OH-3' relative to the C-3' protons are nearly constant [$\sim 55^\circ$ for H-3'(A) and $\sim -55^\circ$ for H-3'(B)]. This is qualitatively consistent with the observed couplings for $J_{3'(A),OH}$ and $J_{3'(B),OH}$.

The envelope forms are found for the 5,6-*O*-isopropylidene rings in a number of models close to the global minimum. This once again implies a discrepancy between the calculated and observed vicinal couplings $J_{5,6}$ and $J_{5,6'}$, similar to that in the case of DE1 models.

Table V lists the observed NOEs for **2** in CDCl₃ and Me₂SO-*d*₆. Although a number of low energy conformers are feasible for **2** at the dielectric of 1.0 (*vide supra*), only two of them (DE1–M1 and DE1–M2) are consistent with the critical NOE between the Me(D) protons and OH-3' proton. Due to the hydrogen bonding between OH-3' and the O-5 of the 5,6-*O*-isopropylidene group, the

TABLE V

Observed NOE data for **2** in CDCl₃ (a) and Me₂SO-*d*₆ (b) qualified as strong (s), medium (m), and weak (w) (see text for discussion). The distances calculated from the models DE1–M1 and DE1–M2 which are the only ones that have the OH-3' proton hydrogen bonded to O-5 consistent with the NOE data. Single values indicate near equality in the two models for the distance parameter. If the values differ by more than 0.1 Å, those corresponding to the DE1–M2 are indicated in parenthesis. In (b) the calculated distances correspond to DE10–M1 and DE10–M2 (indicated in parentheses)

Proton 1		Proton 2	Relative intensity	Calculated distance (Å)
(a)				
H-1	↔	H-2	m	2.5
H-2	↔	H-3	m	2.4
H-2	↔	H-3'(A)	m	2.8
H-3	↔	H-5	m	2.5
H-6	↔	–	H-6'	1.8
H-6	↔	H-5	m	2.4
H-3'(A)	↔	H-3'(B)	s	1.8
H-3	↔	H-3'(A)	m	2.6
H-3'(B)	↔	OH-3'	m	2.3
H-1	↔	Me(A)	w	3.4
H-2	↔	Me(A)	w	3.2
H-4	↔	Me(B)	w	4.1
H-4	↔	H-6'	w	3.8 (3.7)
H-6	↔	Me(C)	w	3.2 (4.5)
H-4	↔	Me(D)	w	4.8 (3.4)
H-5	↔	Me(C)	w	3.3 (4.8)
H-6'	↔	Me(D)	w	4.8 (3.1)
Me(D)	↔	OH-3'	w	3.7 (4.1)
(b)				
H-1	↔	H-2	m	2.5
H-2	↔	H-3	m	2.4
H-5	↔	H-3	m	2.5
H-5	↔	H-4	m	3.1 (2.5)
H-3	↔	OH-3'	w	3.6
H-3'(A)	↔	OH-3'	m	2.3
H-3'(B)	↔	OH-3'	m	2.3
H-6	↔	H-6'	s	1.8
H-6	↔	H-5	m	2.4
H-3'(A)	↔	H-3'(B)	s	1.8
H-1	↔	Me(A)	w	3.4
H-2	↔	Me(A)	w	3.2
H-4	↔	Me(B)	w	4.1
H-5	↔	Me(C)	w	3.5
H-6	↔	Me(C)	w	4.5
H-6'	↔	Me(D)	w	3.6

proton in the former group is located at ~ 3.7 and 4.1 Å from the Me(D) protons in DE1–M1 and DE1–M2, respectively. These distances correspond to a weak NOE as observed in the NMR experiments. The OH-3' proton is separated from Me(D) protons by more than 5 Å in models where the former is hydrogen bonded to O-2 or not hydrogen bonded at all. The observed NOEs in CDCl₃ are thus

qualitatively consistent with the calculated distances in DE1–M1 and DE1–M2. The observed NOEs in Me₂SO-*d*₆ are satisfied by the models in which no intramolecular hydrogen bonding is obtained (e.g., DE1–M4, DE10–M1, DE10–M2, and DE10–M3).

CONCLUSIONS

We have conducted an extensive study of the stereochemical factors concerning the solution structure of the allofuranose **2** in two solvents (CDCl₃ and Me₂SO-*d*₆). The intramolecular and intermolecular electrostatic stabilization (hydrogen bonding) requirements in the two environments are quite different. The NMR and computational results obtained for **2** provide very good qualitative agreement between the observed NMR *J* couplings and NOEs for **2** and the models derived from computational studies. For a dielectric of 1.0 (CDCl₃), the computational study reveals the presence of two low energy models within 1 kcal/mol of the global minimum consistent with the NMR results obtained for **2** in which hydrogen bonding of the OH-3' proton to O-5 is indicated. This is in sharp contrast to the results obtained for the cyanomethyl analog **1** in which there exists a family of low-energy conformations, principally arising as a result of dynamic ring flipping of the 5,6-*O*-isopropylidene ring moiety¹. In the case of **2**, the presence of the intramolecular hydrogen bond from OH-3' to O-5 tends to impart rigidity of the molecule thereby reducing the dynamic conformational averaging of the pendant isopropylidene moiety. The models obtained at the dielectric of 10.0 lack intramolecular hydrogen bonds involving the OH-3' and are presumably dominated by intermolecular hydrogen bonding to the solvent. The conformations of the pendant hydroxymethyl moiety in these models are in general qualitatively consistent with the observed coupling constants for **2** in Me₂SO-*d*₆. This study highlights and further emphasizes the significance and importance of combining both the results of NMR and concurrent computational investigations as a research tool to further reveal insight into the structure and dynamics of molecules in solution.

EXPERIMENTAL

General procedures.—All reactions were carried out at ambient temperature under an Ar atmosphere. The term *in vacuo* refers to concentration first by a rotary evaporator followed by a vacuum pump (< 0.5 torr). Infrared spectra were recorded on a Perkin–Elmer Model 681 grating spectrophotometer (cm⁻¹) for CHCl₃ solutions. Mass spectra were determined on a Finnigan MAT 8430 (0.1 torr NH₃). All NMR spectra were measured using 5-mm o.d. sample tubes (Wilmad-535) containing CDCl₃ or Me₂SO-*d*₆ (Merck Isotopes) solutions at 20°C.

1,2:5,6-Di-O-isopropylidene-α-D-ribo-hexofuranos-3-ulose (4).—To a suspension of 12.9 g (60.0 mmol) of pyridinium chlorochromate and 12.8 g of pulverized 3A molecular sieves in 50 mL of CH₂Cl₂ was added a solution of 1,2:5,6-di-*O*-isopro-

pylidene- α -D-glucofuranose (1 5.20 g; 20.0 mmol) in CH_2Cl_2 (50 mL) dropwise over 45 min to the resulting dark-brown solution. The mixture was stirred for 16 h after which 100 mL of Et_2O was added. After stirring an additional 2 h, the mixture was passed through a column containing 150 g of silica gel topped with 50 g of Celite. Elution with Et_2O followed by concentration in vacuo afforded 4.8 g of a 1:1 mixture of ketone and its corresponding hydrate (89%) as a solid: CIMS, m/z 276 ($\text{M} + \text{NH}_4^+$) and 259 ($\text{M} + \text{H}^+$, 100%); ^1H NMR: δ 6.15 (d, 1 H), 5.83 (d, 1 H), 4.5–3.8 (bm, 12 H), 1.56 (s, 3H), 1.46 (s, 3 H), 1.43 (s, 3 H), 1.42 (s, 3 H), 1.37 (s, 3 H), 1.33 (s, 3 H), and 1.30 (s, 3 H); ^{13}C NMR (CDCl_3): δ 208.0, 114.1, 113.1, 110.2, 109.7, 104.0, 102.8, 100.7, 83.4, 78.6, 78.5, 76.0, 73.7, 66.5, 64.0, 27.2, 26.8, 26.6, 26.3, 25.6, 25.0, and 24.8. Anal. Calcd for $\text{C}_{12}\text{H}_{18}\text{O}_6 \cdot 0.5 \text{H}_2\text{O}$: C, 53.93; H, 7.15. Found C, 54.21; H, 7.39.

*3-Deoxy-1,2 : 5,6-di-O-isopropylidene-3-C-(methylene)- α -D-glucofuranose*² (5).—To magnesium turnings (2.0 g, 83 mmol) in dry ether (150 mL) was added a few drops of 1,2-dibromoethylene at room temperature to initiate the Grignard reaction. Chloromethyltrimethylsilane (11 mL, 79 mmol) was added at a rate so that a gentle reflux was maintained. After refluxing the suspension for 2 h followed by cooling to room temperature, an ethereal solution (50 mL) of 4 (8.7 g, 34 mmol) was added and the mixture stirred for 2 days. The mixture was then poured into satd aq NH_4Cl and separated. The aqueous layer was extracted with Et_2O ($2 \times$), the organic phases combined and washed with brine, dried (MgSO_4) and concentrated in vacuo affording the crude silyl alcohol as a fluffy white solid (10 g, 85%) which was used without further purification; ^1H NMR: δ 5.55 (d, 1 H), 4.13 (d, 1 H), 4.08–3.90 (m, 2 H), 3.80 (dd, 1 H), 3.63 (d, 1 H), 2.48 (s, 1 H), 1.45 (s, 3 H), 1.30 (s, 3 H), 1.22 (2 s, 6 H), 1.00 (d, 1 H), 0.50 (d, 1 H), and 0.01 (s, 9 H); ^{13}C NMR: δ 112.1, 108.8, 103.2, 82.8, 82.3, 79.2, 73.2, 66.9, 26.1, 25.9, 24.7, 20.1, and 0.0.

To a suspension of a 60% dispersion of NaH (7.4 g, 185 mmol; prewashed $4 \times$ with hexane) in THF (110 mL) cooled in an ice bath was added a solution of the crude silyl alcohol (10.4 g, 30.1 mmol) in THF (100 mL) dropwise. The mixture was refluxed for 6 h, cooled to room temperature and excess hydride decomposed by the addition of satd aq NH_4Cl . After separating the layers, the aqueous layer was extracted with Et_2O ($2 \times$), the organic phases combined and washed with brine, dried (MgSO_4), and concentrated in vacuo to afford 7.5 g (97%) of 5 (ref 2) as a pale-yellow liquid which was used without further purification; ^1H NMR: δ 5.81 (d, 1 H), 5.51 (1 H), 5.47 (m, 1 H), 4.89 (dd, 1 H), 4.65 (m, 1 H), 4.10–4.02 (bm, 2 H), 3.98–3.90 (m, 1 H), 1.52 (s, 3 H), 1.43 (s, 3 H), and 1.37 (2s, 6 H); ^{13}C NMR: δ 146.9, 113.4, 112.6, 109.8, 104.6, 82.2, 79.3, 77.4, 65.8, 27.4, 27.1, 26.6, and 25.5.

3-Deoxy-3-C-(hydroxymethyl)-1,2 : 5,6-di-O-isopropylidene- α -D-allofuranose^{2,4} (2).—The foregoing compound (7.5 g, 29.3 mmol) was dissolved in dry THF (150 mL) and the solution cooled to 0°C . Borane–methyl sulfide complex (2 M, 22 mL; 44.0 mmol) was added dropwise and the solution stirred at room temperature for 16 h. After cooling to 0°C , 50% aq THF (32 mL), 2 M aq NaOH (93 mL) and 30% H_2O_2 (102 mL) were added successively. After stirring at room temperature for 2 days

water (100 mL) and EtOAc (100 mL) were added and the layers separated. The aqueous phase was extracted with EtOAc, the organic phases combined and washed with brine, dried (MgSO_4) and concentrated in vacuo. Purification by column chromatography (silica gel, 40% EtOAc–hexane) afforded 6.0 g (75%) of **2** (refs 2,4) as a pale-yellow liquid: $[\alpha]_{25}^D$: +29.0 (c 1.07, CHCl_3); IR 3470, 2990, and 2860; CIMS m/z 273 ($\text{M} - \text{H}^+$) and 234; ^1H NMR data for **2** are summarized in Tables I and II. The ^{13}C NMR data for **2** are summarized in Table III. Anal. Calcd for $\text{C}_{13}\text{H}_{22}\text{O}_6 \cdot 0.2 \text{H}_2\text{O}$: C, 56.18, H, 8.12. Found: C, 55.86; H, 7.96.

NMR spectroscopy.—One-dimensional ^1H and ^{13}C NMR spectra were collected by using either a Varian VXR-400 spectrometer operating at 400 and 100 MHz, respectively, or a General Electric QE-300 spectrometer operating at 300 and 75 MHz, respectively. All two-dimensional NMR spectra were collected with the VXR-400 which was equipped with a 5-mm broad-band (BB) switchable probe and variable temperature accessory. One-dimensional proton data were routinely processed with a 65K data-table (0.09 Hz/pt); for additional accuracy the data were processed with a 128K data table (0.046 = Hz/pt).

Phase-sensitive double quantum filtered COSY (DQF-COSY).—The general experimental parameters used for collecting DQF-COSY data for **2** in CDCl_3 were as follows: sequence, D1–(90)– t_1 –(90)(90)–acquire(t_2); relaxation delay (D1), 11 s; acquisition time (t_2), 332 ms; the number of data points in F2 was 2048 and the number of increments was 2×256 , employing the States–Haberkorn–Reuben hypercomplex data-collection and data-processing scheme⁶; the number of transient, 32/increment with steady-state pulses, 2; the data were processed with line-broadening of 0.1 Hz in both t_1 and t_2 domains, respectively; the data points in t_1 were zero-filled to 2048 points prior to Fourier transformation and the final data set was symmetrized.

Absolute-value COSY-4 (90–90).—The general experimental parameters for collecting the absolute value COSY data for **2** in $\text{Me}_2\text{SO}-d_6$ are as follows: sequence, D1–(90)– t_1 –(90)–acquire(t_2); relaxation delay (D1), 1 s; acquisition time (t_2), 351 ms; number of data points collected in F2, 2048; number of increments in t_1 , 256; the final data set was zero-filled to 2048×2048 data points, with pseudo-echo weighting of the fid's in both time domains prior to Fourier transformation with symmetrization and absolute value display.

Phase-sensitive NOESY.—The data-acquisition parameters used for **2** were as follows: sequence, D1–(90)– t_1 –(90)–MIX–(90)–acquire(t_2); relaxation delay (D1), 11 s; mixing time (MIX), 1.0 s. The line-broadening and data processing scheme including symmetrization were the same as for the DQF-COSY experiment. Concerning the plotted NOESY data for **2** shown in Figs. 1 and 2, positive contours (NOE) are plotted with full (10) contours (dark); negative contours (diagonal and in-phase chemical exchange cross-peaks) are plotted as single contours (open circles).

^1H – ^{13}C -Heteronuclear shift correlation (HETCOR).—The acquisition parameters used for **2** are as follows: sequence, D1–(90)(H)– $t_1/2$ –BIRD pulse (H,

C)– $t_1/2$ –(90)(H, C)–acquire(t_2); relaxation delay (D1), 2.0 s; acquisition time (t_2), 58 ms; $^1J_{CH}$, 140 Hz (average value for direct 1-bond coupling); the number of data points in the carbon dimension (F2) was 1216 points and the number of increments was 128 or 256. Both dimensions were zero-filled to 2048×2048 points in both time domains with pseudo-echo weighting prior to Fourier transformation with absolute value display in the frequency domain.

Proton homonuclear 2D J-spectroscopy.—The experimental parameters used for collecting the homonuclear 2D *J*-spectra on **2** are as follows: sequence, D1–(90)– $t_1/2$ –(180)– $t_1/2$ –acquire(t_2); relaxation delay (D1), 4 s; spectral window in (F2), 3085.5 Hz; acquisition time, 332 ms; number of points collected in F2, 2048; spectral window in (F1), 50 Hz, and number of increments, 512. The data points in F1 were zero-filled to 2048 points with pseudo-echo weighting optimized for resolution applied to the time domain fid's prior to Fourier transformation with absolute value display.

Molecular modeling.—Molecular modeling studies were carried out on **2** with a view to determining its energetically favored conformations and to determine if the conformational characteristics of the low energy minima correlate with the NMR derived distances (NOE) and torsion angles (vicinal proton–proton coupling constants). In order to achieve this end, it was necessary to exhaustively investigate the conformations possible for these compounds and to determine which low energy conformations fit the experimental data. In particular, the flexibility due to the pseudorotation in the five-membered rings deserves attention.

A preliminary model of **2** was built using the computer graphics package MacroModel¹⁴ and refined using a combination of steepest descent, block diagonalized Newton–Raphson, and full matrix Newton–Raphson minimization techniques, with a dielectric of 1.0. Throughout the study the force field used was the MacroModel version of MM2.

A set consisting of 27360 starting conformations of **2** was generated and energy minimized using MacroModel*. These incorporated (a) the rotational flexibility about the C-3–C-3' and C-4–C-5 bonds, (b) the pseudorotation of the 5,6-*O*-isopropylidene ring, and the [3.3.0] ring system. Conformations higher than 7 kcal/mol in energy relative to the global minimum were eliminated from further consideration. For reasons stated earlier, the final sets of energy refined models were obtained at the dielectrics of 1.0 and 10.0. These were arranged in ascending order of energy and viewed and analyzed graphically using SYBYL**. Conformational energy calculations were performed wherein energies were computed as a function of the torsions about the C-4–C-5 (χ_1) and C-3–C-3' (χ_2) bonds using the MM2

* The MacroModel Program (version 2.5) was modified by Dr. Dale Spangler, Drug Design of Searle Research and Development, to incorporate the option of keeping torsion angles fixed (FIXT) during energy optimizations in the Batchmin module.

** SYBYL version 5.32. Molecular modeling software developed and released by Tripos Associates, Inc. Copyright 1986, 1989, and 1990.

and MM3 force fields as implemented in MacroModel (v3.5). A collection of 324 conformations of **2** was generated by starting from DE1–M1 and varying the two torsions at 20° interval. This collection was energy-minimized with constraints of 1000 kcal/mol on the two torsions with the rest of **2** being allowed to optimize in cartesian space. The energies were then plotted in the χ_1 – χ_2 conformational space using the Deltagraph software on Macintosh, Isoenergy contours were drawn at 1 kcal/mol interval starting from the global minimum (marked as 0). Contours of value greater than 6 kcal/mol relative to the global minimum are not shown.

ACKNOWLEDGMENTS

Microanalytical determinations were performed by the Physical Methodology Department at Searle. We acknowledge Ms. Lilian Garcia for her assistance in obtaining the NMR data described here. We thank Professor G.W.J. Fleet and Mr. D.R. Witty (Oxford University) for sharing a preprint of their work². We are very grateful to Dr. Dale Spangler of Drug Design and Mr. Dan Volocyk of SMIS for their intense efforts in the port of the Batchmin module in MacroModel to the parallel computing environment of Intel Hypercube together with the development of a user-friendly interface. The authors acknowledge Dorothy Ryno and Nilde Del Castillo of Searle Information Services for their assistance.

REFERENCES

- 1 D.C. Lankin, S.T. Nugent, and S.N. Rao, *Carbohydr. Res.*, 229 (1992) 245–269.
- 2 F.X. Wilson, G.W.J. Fleet, K. Vogt, D.R. Witty, S. Choi, R. Storer, P.L. Meyers, and C.J. Wallis, *Tetrahedron Lett.*, 47 (1990) 6931–6934.
- 3 D.J. Peterson, *J. Org. Chem.*, 33 (1968) 780–784.
- 4 (a) A. Rosenthal and D.A. Baker, *J. Org. Chem.*, 38 (1973) 193–197. (b) D.C. Baker, D. Horton, and C.G. Tindall, Jr., *Methods Carbohydr. Chem.*, 7 (1976) 3–6.
- 5 U. Piantini, O.W. Sorensen, and R.R. Ernst, *J. Am. Chem. Soc.*, 104 (1982) 6800–6801. (b) G.E. Martin, A.S. Zektzer, *Two-Dimensional NMR Methods for Establishing Molecular Connectivity: A Chemist's Guide to Experiment Selection, Performance, and Interpretation*, VCH, New York, 1988, pp 58–161.
- 6 (a) D.J. States, R.A. Haberhorn and D.J. Ruben, *J. Magn. Reson.*, 48 (1982) 286–292. (b) D. Neuhaus, and M. Williamson, *The Nuclear Overhauser Effect in Stereochemical and Conformational Analysis*, VCH, New York, 1989.
- 7 S.L. Patt and J.N. Shoolery, *J. Magn. Reson.*, 46 (1982) 535–539.
- 8 (a) A. Bax and G.A. Morris, *J. Magn. Reson.*, 42 (1981) 501–505. (b) A. Bax, *J. Magn. Reson.*, 53 (1983) 517–520.
- 9 N.L. Allinger, Y.H. Yuh, and J.-H. Lii, *J. Am. Chem. Soc.*, 111 (1989) 8551–8566.
- 10 N.L. Allinger, M. Rahman, and J.-H. Lii, *J. Am. Chem. Soc.*, 112 (1990) 8293–8307.
- 11 C.A.G. Haasnoot, F.A.A.M. de Leeuw, and C. Altona, *Tetrahedron*, 36 (1980) 2783–2792.
- 12 R.C. Cookson, T.A. Crabb, J.J. Frankel, and J. Hudec, *Tetrahedron, Suppl. No. 7*, (1966) 355–390.
- 13 R. Cahill, R.C. Cookson, and T.A. Crabb, *Tetrahedron*, 25 (1969) 4681–4709.
- 14 R. Cahill, R.C. Cookson, and T.A. Crabb, *Tetrahedron*, 25 (1969) 4711–4735.
- 15 M. Barfield and W.B. Smith, *J. Am. Chem. Soc.*, 114 (1992) 1574–1581.
- 16 A. De Bruyn, D. Danneels, M. Anteunis, and E. Saman, *J. Carbohydr. Nucleos. Nucleot.*, 2 (1975) 227–240.
- 17 C. Landis and V.S. Allured, *J. Am. Chem. Soc.*, 113 (1991) 9493–9499.
- 18 F. Mohamadi, N.G.J. Richards, W.C. Guida, R. Liskamp, M. Lipton, C. Caulfield, G. Chang, T. Hendrickson, and W.C. Still, *J. Comp. Chem.*, 11 (1990) 440–467.